Features due to spin-orbit coupling in the optical conductivity of single-layer graphene

P. Ingenhoven,[1] J. Z. Bernád,[1] U. Zülicke,[1,2] and R. Egger[3]

[1]*Institute of Fundamental Sciences and MacDiarmid Institute for Advanced Materials and Nanotechnology, Massey University, Manawatu Campus, Private Bag 11 222, Palmerston North 4442, New Zealand*

[2]*Centre for Theoretical Chemistry and Physics, Massey University, Albany Campus, Private Bag 102904, North Shore MSC, Auckland 0745, New Zealand*

[3]*Institut für Theoretische Physik, Heinrich-Heine-Universität, D-40225 Düsseldorf, Germany*

(Received 4 November 2009; revised manuscript received 21 December 2009; published 21 January 2010)

We have calculated the optical conductivity of a disorder-free single graphene sheet in the presence of spin-orbit coupling, using the Kubo formalism. Both intrinsic and structural-inversion-asymmetry induced types of spin splitting are considered within a low-energy continuum theory. Analytical results are obtained that allow us to identify distinct features arising from spin-orbit couplings. We point out how optical-conductivity measurements could offer a way to determine the strengths of spin splitting due to various origins in graphene.

DOI: 10.1103/PhysRevB.81.035421 PACS number(s): 81.05.U−, 72.10.Bg, 71.70.Ej

I. INTRODUCTION

Graphene is a single sheet of carbon atoms forming a two-dimensional honeycomb lattice. This material has only recently become available for experimental study, and its exotic physical properties have spurred a lot of interest.[1,2] Known theoretically since the late 40s,[3] graphene is a promising candidate for applications due to its excellent mechanical properties,[4] scalability down to nanometer sizes,[5] and exceptional electronic properties.[6] The conical shape of conduction and valence bands near the K and K' points in the Brillouin zone renders graphene an interesting type of quasirelativistic condensed-matter system[7,8] where mass-less Dirac-fermion-like quasiparticles are present at low energy. In contrast to the truly relativistic case, the spin degree of freedom in their Dirac equation corresponds to a pseudospin that distinguishes degenerate states on two sublattices formed by two nonequivalent atom sites present in the unit cell.

The pseudospin degeneracy can be broken by spin-orbit interaction (SOI), which mixes pseudospin and real spin. There has been huge interest in SOI in graphene, resulting in a large body of theoretical[9–24] and experimental[25–29] work. There are two main causes for the SOI in graphene. First, external electric fields (e.g., due to the presence of a substrate, a backgate, or adatoms) and local curvature fields (ripples) induce a SOI (Refs. 12–14, 20, and 24) whose coupling strength we denote by Δ_R. We refer to this contribution as the *Rashba* SOI in the following. In addition, there is an *intrinsic* SOI (Refs. 9, 12–16, and 24) with strength Δ_I, which is caused by the atomic Coulomb potentials.

Existence of the intrinsic and Rashba SOIs can be inferred from group-theoretical arguments.[9,12,20] However, the actual values of their respective strengths Δ_R and Δ_I are the subject of recent debate. Initial estimates[12] have been refined using tight-binding models[13,14] and density-functional calculations.[15,16,24] First experimental observations of spin-orbit-related effects in graphene's band structure based on angle resolved photoemission spectroscopy data[26,27] have later been questioned.[28,29] Detailed knowledge about typical magnitudes and ways to influence Δ_R and Δ_I is crucial, e.g., for understanding spin-dependent transport[30] and spin-based quantum devices[31] in graphene. The desire to identify possible alternative means of observing, and measuring, spin-orbit coupling strengths in graphene has provided the motivation for our work reported here.

We present a theoretical analysis of graphene's optical conductivity $\sigma(\omega)$, extending previous studies[32–40] to the situation with finite SOI. SOI effects on the DC conductivity were investigated in a recent theoretical study for a bipolar graphene *pn* junction,[41] and the effect of intrinsic SOI on the polarization-dependent optical absorption of graphene was considered in Ref. 42. Our study presents the analogous scenario for the richer case of the optical conductivity when both intrinsic and extrinsic types of SOI are present. Since Δ_R can be tuned by external fields, we will analyze various situations distinguished by the relative strengths of Δ_R and Δ_I.

Our findings suggest that optical-conductivity measurements can be useful to identify and separate different SOI sources. We work on the simplest theory level (linear-response theory, no interactions, no disorder) and disregard boundary effects for the moment. The structure of the remainder of this paper is as follows. In Sec. II, we summarize basics of our calculation of the optical conductivity based on the Kubo formalism; except for some details that have been relegated to the Appendix. In Sec. III, we show results for different relative magnitudes of SOI strengths at finite temperature T and chemical potential μ. Finally, in Sec. IV, we summarize our results and discuss their applicability to actual experiments.

II. OPTICAL CONDUCTIVITY

We start from a low-energy continuum description of graphene,[6] $H(\mathbf{k})=H_0(\mathbf{k})+H_R+H_I$. Without the SOI terms H_R and H_I, the single-particle Hamiltonian in plane-wave representation reads as

$$H_0(\mathbf{k}) = \hbar v(k_x\sigma_x + k_y\tau_z\sigma_y), \tag{1}$$

with Fermi velocity $v \approx 10^6$ m/s. The Pauli matrices $\sigma_{x,y}$ act in pseudospin space, where the two eigenspinors of σ_z cor-

respond to quasiparticle states localized on sites of the A and B sublattice. Analogous Pauli matrices $\tau_{x,y,z}$ act in the two-valley space spanned by states near the two K points. The part of the effective Hamiltonian describing Rashba SOI is given by

$$H_R = \frac{\Delta_R}{2}(\sigma_x \tau_z s_y - \sigma_y s_x), \tag{2}$$

where Δ_R includes both the external electric-field and curvature effects in a coarse-grained approximation, with the latter assumed to be homogeneous. The Pauli matrices $s_{x,y,z}$ act in the real spin space. For the intrinsic SOI induced by atomic potentials, we have

$$H_I = \Delta_I \sigma_z \tau_z s_z. \tag{3}$$

The full Hamiltonian is then an 8×8 matrix in the combined sublattice, spin, and valley space.

The full Hamiltonian matrix turns out to be block-diagonal in the valley degree of freedom, and each block can be transformed into the other via a unitary transformation. The bulk spectrum—ignoring subtleties related to the topological insulator phase encountered for $2\Delta_I > \Delta_R$ (Ref. 12) for now—can then be obtained from a 4×4 Hamiltonian matrix in the basis $(A\uparrow, B\uparrow, A\downarrow, B\downarrow)$ at one K point. The valley degree of freedom then merely manifests itself as a degeneracy factor $g_v=2$. The energy spectrum is obtained as

$$\varepsilon_{\mathbf{k},\nu\nu'} = \frac{1}{2}(\nu'\Delta_R + \nu\sqrt{4(\hbar v)^2|\mathbf{k}|^2 + (\Delta_R - 2\nu'\Delta_I)^2}), \tag{4}$$

where the combined indices $\nu, \nu' = \pm 1$ label the four bands. The corresponding eigenstates

$$|n\rangle = |\mathbf{k}\rangle \otimes |\nu\nu'\rangle_{\mathbf{k}} \tag{5}$$

are composed of a plane-wave state $|\mathbf{k}\rangle$ and a $\mathbf{k}$-dependent 4-spinor $|\nu\nu'\rangle_{\mathbf{k}}$.

We compute the optical conductivity using the standard Kubo formula,[43]

$$\sigma_{ab} = \int_{-\infty}^{0} dt e^{i(\omega - i0^+)t} K_{ab}(t), \tag{6}$$

where $a,b=x,y$ and the kernel reads as

$$K_{ab} = \frac{ie}{\hbar}\mathrm{Tr}\{e^{-i/\hbar H(\mathbf{k})t} j_a e^{i/\hbar H(\mathbf{k})t}[r_b, \rho_0]\}. \tag{7}$$

Here e denotes the electron charge, r_b is a Cartesian component of the position operator, ρ_0 the equilibrium density matrix, and the current operators are given by

$$j_a = \frac{ie}{\hbar}[H(\mathbf{k}), r_a] = \frac{e}{\hbar}\frac{\partial H(\mathbf{k})}{\partial k_a}. \tag{8}$$

Following Ref. 32, we use the single-particle eigenstates $|n\rangle$ and eigenenergies ε_n. The conductivity then reads as

$$\sigma_{ab}(\omega) = \frac{e^2}{i}\sum_{n,n'} \frac{\langle n|[H,r_a]|n'\rangle\langle n'|[H,r_b]|n\rangle}{(\varepsilon_{n'} - \varepsilon_n)(\varepsilon_{n'} - \varepsilon_n + \hbar\omega - i0^+)} \times [f(\varepsilon_n) - f(\varepsilon_{n'})], \tag{9}$$

where $f(\varepsilon)$ is the Fermi-Dirac distribution containing the chemical potential μ and the inverse temperature $\beta = 1/(k_B T)$.

In the absence of a magnetic field, the off-diagonal entries vanish, $\sigma_{xy}=0$, while symmetry arguments show that $\sigma_{xx}=\sigma_{yy}\equiv\sigma(\omega)$. At finite ω in the clean system, only the interband contribution to the conductivity is relevant. Its real part is given by

$$\mathrm{Re}\,\sigma(\omega) = \pi e^2 \int \frac{d^2\mathbf{k}}{(2\pi)^2}{\sum}' |w^a_{\kappa\nu,\kappa'\nu'}(\mathbf{k})|^2 \frac{f(\varepsilon_{\mathbf{k},\kappa\nu}) - f(\varepsilon_{\mathbf{k},\kappa'\nu'})}{\varepsilon_{\mathbf{k},\kappa'\nu'} - \varepsilon_{\mathbf{k},\kappa\nu}} \times [\delta(\varepsilon_{\mathbf{k},\kappa\nu} - \varepsilon_{\mathbf{k},\kappa'\nu'} + \hbar\omega) + \delta(\varepsilon_{\mathbf{k}\kappa'\nu'} - \varepsilon_{\mathbf{k}\kappa\nu} + \hbar\omega)], \tag{10}$$

where

$$w^a_{\kappa\nu,\kappa'\nu'}(\mathbf{k}) = {}_{\mathbf{k}}\langle\kappa\nu|j_a|\kappa'\nu'\rangle_{\mathbf{k}}$$

are the current operator matrix elements in the eigenbasis, and $\Sigma' = \Sigma_{(\kappa\nu)\neq(\kappa'\nu')}$. We also used

$$w^a_{\kappa\nu,\kappa'\nu'}(\mathbf{k}) = [w^a_{\kappa'\nu',\kappa\nu}(\mathbf{k})]^\dagger$$

since the current operator is Hermitian. In what follows, we restrict ourselves to the real part of $\sigma(\omega)$ and omit the "Re" sign.

The result obtained for $\omega > 0$ can be expressed very generally as

$$\frac{\sigma(\omega)}{\sigma_0} = 2\pi\sum_{n=1}^{6} F_n(\omega, \Delta_R, \Delta_I, \beta, \mu), \tag{11}$$

where $\sigma_0 = g_v e^2/(2\pi\hbar)$ and, with the Heaviside function Θ, the quantities F_n are given by

$$F_1 = \tilde{F}_1 \Theta(\hbar\omega - |\Delta_R - 2\Delta_I|),$$

$$F_2 = \tilde{F}_2[\Theta(\Delta_R - 2\Delta_I)\Theta(\hbar\omega - \Delta_R)\Theta(2\Delta_I + \Delta_R - \hbar\omega) + \Theta(2\Delta_I - \Delta_R)\Theta(\hbar\omega - \Delta_R)\Theta(2\Delta_R - \hbar\omega)],$$

$$F_3 = \tilde{F}_3[\Theta(\Delta_R - 2\Delta_I) + \Theta(2\Delta_I - \Delta_R)\Theta(\hbar\omega - 2\Delta_I + \Delta_R)],$$

$$F_4 = \tilde{F}_4[\Theta(\Delta_R - 2\Delta_I)\Theta(\hbar\omega - 2\Delta_R) + \Theta(2\Delta_I - \Delta_R)\Theta(\hbar\omega - 2\Delta_I - \Delta_R)],$$

$$F_5 = \tilde{F}_5[\Theta(\Delta_R - 2\Delta_I)\Theta(\hbar\omega - \Delta_R + 2\Delta_I)\Theta(\Delta_R - \hbar\omega) + \Theta(2\Delta_I - \Delta_R)\Theta(\Delta_R - \hbar\omega)],$$

$$F_6 = \tilde{F}_6 \Theta(\hbar\omega - 2\Delta_I - \Delta_R). \tag{12}$$

The rather lengthy analytical expressions for the quantities $\tilde{F}_n(\omega, \Delta_R, \Delta_I, \beta, \mu)$ can be found in the Appendix.

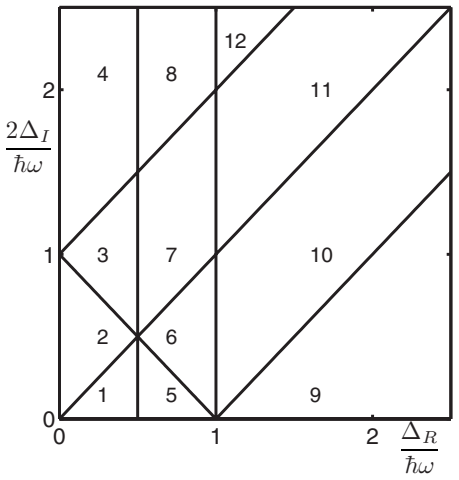

FIG. 1. Regions in the $\Delta_R/\hbar\omega-2\Delta_I/\hbar\omega$-plane where the different $\tilde{F}_n$ contribute (cf. Table I). There is no contribution to $\sigma(\omega)$ from region 4.

Figure 1, in conjunction with Table I, shows the regions in the $\Delta_R/\hbar\omega-2\Delta_I/\hbar\omega$ plane where the different $\tilde{F}_n$ contribute.

III. RESULTS

We now discuss the main physical observations arising from Eqs. (11) and (12). First, the behavior of the conductivity is qualitatively different in the two regimes $\Delta_R>2\Delta_I$ and $\Delta_R<2\Delta_I$. It is well known that the latter regime corresponds to a topological insulator phase while the former yields a conventional band insulator, with a quantum phase transition in between. For the topological insulator phase,[12,44–46] spin-polarized gapless edge states forming a helical liquid will dominate the optical conductivity when both k_BT and $\hbar\omega$ are smaller than the gap energy. In that regime, the conductivity is expected[12] to exhibit power-law behavior analogous to that found for ordinary one-dimensional electron systems.[47,48] In what follows, we consider the frequency and temperature range such that the optical conductivity is still mostly determined by the bulk states.

Sharp features are exhibited by the conductivity as a function of frequency ω, which depend on the relative strength of the two SOI terms and should therefore allow for a clear identification of these couplings. We start by discussing a few special cases. For $\Delta_R=0$ but finite Δ_I, the gapped spectrum consisting of two doubly (spin-)degenerate dispersion branches leads to a vanishing conductivity for $\hbar\omega<\Delta_I$, and all other features expected in the presence of a generic mass gap.[33,39] In contrast, for $\Delta_I=0$ but finite Δ_R, the band structure mimics that of bilayer graphene, only with a gap smaller by up to 4 orders of magnitude.[9,49] The optical conductivity for this case has the same functional form as the conductivity for bilayer graphene[37,40] except that the McClure[49] interlayer hopping constant is replaced by Δ_R. In particular, it exhibits a δ-peak at $\hbar\omega=\Delta_R$ and a kink at $\hbar\omega=2\Delta_R$. With $\hbar vk=\varepsilon$, the analytical expression is

$$\frac{\sigma}{\sigma_0}=\frac{\pi}{2}\delta(\hbar\omega-\Delta_R)\int_0^\infty d\epsilon\frac{\epsilon\Delta_R}{4\epsilon^2+\Delta_R^2}\times\left[g\left(\frac{1}{2}(\Delta_R+\sqrt{4\epsilon^2+\Delta_R^2})\right)+g\left(\frac{1}{2}(\Delta_R-\sqrt{4\epsilon^2+\Delta_R^2})\right)\right]+\frac{\pi}{8}g\left(\frac{\hbar\omega}{2}\right)\left[\frac{\hbar\omega+2\Delta_R}{\hbar\omega+\Delta_R}+\frac{\hbar\omega-2\Delta_R}{\hbar\omega-\Delta_R}\Theta(\hbar\omega-2\Delta_R)\right]+\frac{\pi}{8}\frac{\Delta_R^2}{(\hbar\omega)^2}\left[g\left(\frac{\hbar\omega+\Delta_R}{2}\right)+g\left(\frac{\hbar\omega-\Delta_R}{2}\right)\right]\Theta(\hbar\omega-\Delta_R),\tag{13}$$

where we define the function

$$g(\varepsilon)=\frac{\sinh(\varepsilon\beta)}{\cosh(\mu\beta)+\cosh(\varepsilon\beta)}.\tag{14}$$

In the limit $\Delta_R=\Delta_I=0$, the optical conductivity of clean graphene with its spin-degenerate linear dispersion is recovered.[34,35] The asymptotic behavior for large frequencies turns out to be independent of the SOI couplings, with σ always approaching the well known universal value $e^2/(4\hbar)$.

The optical conductivity for various situations where both Δ_R and Δ_I are finite is shown next in a series of figures. In particular, Fig. 2 shows the case where $\Delta_R>2\Delta_I$. In Fig. 3, we are at the special point $\Delta_R=2\Delta_I$. Furthermore, Fig. 4 illustrates the regime where $\Delta_R<2\Delta_I$. To be specific, all these figures are for $T=1$ K. Finally, Fig. 5 displays the effects of thermal smearing.

TABLE I. List of $\tilde{F}_n$ functions and the regions in which they contribute, as illustrated in Fig. 1.

$\tilde{F}_1$	$\tilde{F}_2$	$\tilde{F}_3$	$\tilde{F}_4$	$\tilde{F}_5$	$\tilde{F}_6$
1–3, 5–7, 10, 11	6–8	1–3, 5–7, 9–11	1, 2	10–12	1, 2, 5

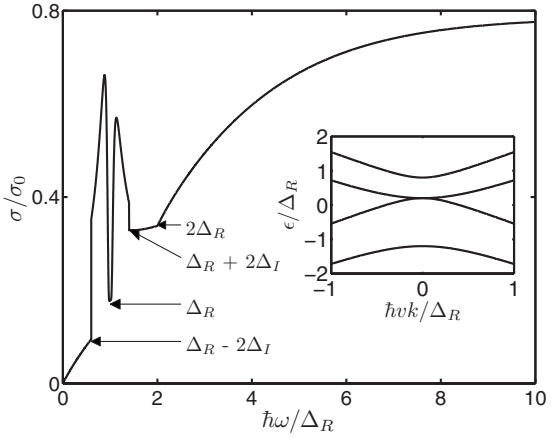

FIG. 2. Optical conductivity at $T=1$ K for graphene with $\Delta_R=100$ μeV and $\Delta_I=0.2\Delta_R$, thus realizing the case $2\Delta_I<\Delta_R$. We set $\mu=\Delta_I$ to maintain charge neutrality. Inset: Low-energy part of the bandstructure. Kinks in the frequency dependence of σ arise when new transitions between different bands become possible at certain critical values of ω.

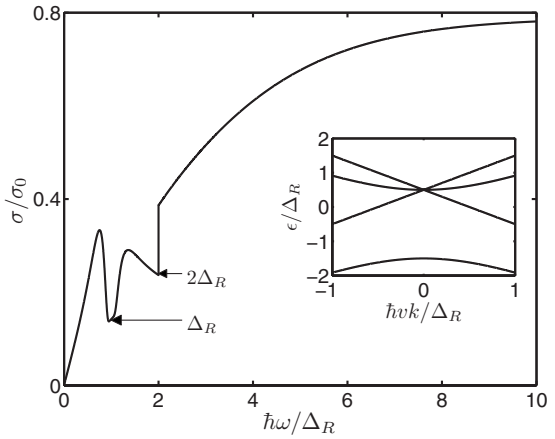

FIG. 3. Optical conductivity at $T=1$ K for graphene obtained for the special case $2\Delta_I=\Delta_R$ with $\Delta_R=100$ μeV, setting $\mu=\Delta_I\equiv\Delta_R/2$ to ensure charge neutrality. Inset: The bandstructure shows that three bands cross at $k=0$ and, hence, some of the kinks present in Fig. 2 disappear.

For $2\Delta_I<\Delta_R$, we observe a splitting and widening of the δ peak at Δ_R, while the kink at $2\Delta_R$ stays at the same position. In addition, we observe kinks at $\Delta_R\pm2\Delta_I$ (see Fig. 2). At the quantum phase-transition point $2\Delta_I=\Delta_R$, the dispersion exhibits a crossing of two massless branches with a massive branch, see inset of Fig. 3. As a consequence, certain sharp features exhibited by the optical conductivity in other cases disappear. For $2\Delta_I>\Delta_R$, see Fig. 4, the conductivity shows kinks at $\hbar\omega=\Delta_R$, at $\hbar\omega=2\Delta_R$, and at $2\Delta_I\pm\Delta_R$.

We have chosen to show a very wide range of SOI parameters Δ_R and Δ_I in these figures. Previous estimates for these parameters[12–16,24] range from 0.5 to 100 μeV for Δ_I, and 0.04 to 23 μeV for Δ_R. The Rashba coupling is expected to be linear in the electric backgate field, with proportionality constant 10 μeV nm/V,[24] allowing for an experimental lever to sweep through a wide parameter range. On the experimental side, the picture is currently mixed. One recent experimental study[25] finds $\Delta_R=370$ μeV (210 μeV) for electrons (holes) in carbon nanotubes. A much larger value $\Delta_R=13$ meV has been reported for graphene sheets fabricated on a nickel surface.[27]

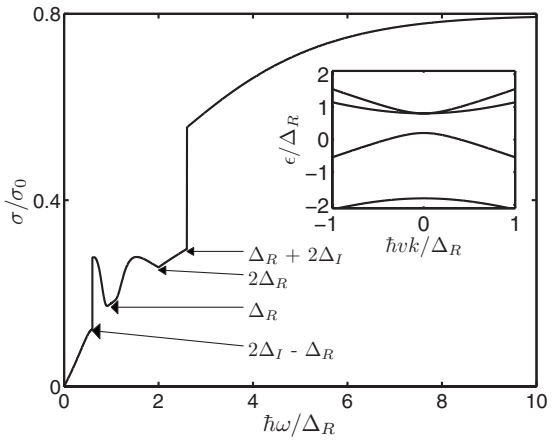

FIG. 4. Same as Fig. 2, except that $\Delta_I=0.8\Delta_R$ with $\Delta_R=100$ μeV, thus realizing the case $2\Delta_I>\Delta_R$. Charge neutrality is maintained by setting $\mu=\Delta_R/2$.

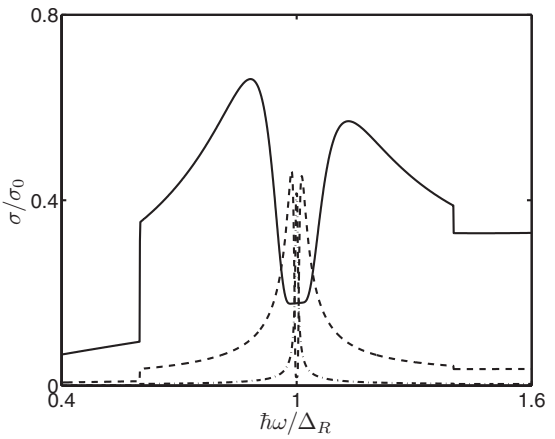

FIG. 5. Same as Fig. 2, focusing on the region $0.4<\hbar\omega/\Delta_R<1.6$. The solid curve is for $T=1$ K, the dashed curve for $T=10$ K, and the dot-dashed one for $T=100$ K. The distinct kinks are thermally smeared and suppressed at elevated temperatures, but remain visible up to $T\approx10$ K.

For low temperatures (e.g., at $T=1$ K in the above figures), the SOI couplings can be distinguished by the different peak structures appearing in the optical conductivity. Increasing the temperature leads to thermal smearing of those features, as illustrated in Fig. 5. However, the characteristic SOI-induced peak and kink features should still be visible in the optical conductivity up to $T\approx10$ K, albeit with a smaller magnitude.

IV. CONCLUSIONS

We have calculated the optical conductivity for a graphene monolayer including the two most relevant spin-orbit couplings, namely the intrinsic atomic contribution Δ_I and the curvature- and electric-field-induced Rashba term Δ_R. Our result for the optical conductivity, which we presented for finite temperature and chemical potential, shows kinks and/or peaks at frequencies corresponding to Δ_R, $2\Delta_R$, and $|\Delta_R\pm2\Delta_I|$. Measuring the optical conductivity in a frequency range covering these energy scales can be expected to yield detailed insights into the nature of spin-orbit interactions in graphene.

We did not analyze disorder effects but expect all sharp features to broaden since the δ functions in Eq. (10) effectively become Lorentzian peaks. We also did not consider the effect of electron-electron interactions. While renormalization-group studies indicate that weak unscreened interactions are marginally irrelevant,[6] interactions may still play an important role. For instance, Ref. 50 considers interaction effects on the optical properties of doped graphene without spin-orbit coupling. Interactions cause interband (optical) and intraband (Drude) transitions and thus a finite DC conductivity. We expect that the peak and kink structures arising from the spin-orbit couplings survive, however, because the relevant contributions are additive.

Recent experimental studies suggest that an optical measurement of the conductivity in the energy range relevant for SOI should be possible. Fei *et al.*[51] measured the optical

conductivity from $\hbar\omega = 1.54$ eV up to 4.13 eV. Slightly lower energies (0.2–1.2 eV) were reached in Ref. 52. We suggest to perform low-temperature experiments at microwave frequencies, with energies ranging from several μeV to a few meV.

ACKNOWLEDGMENTS

Useful discussions with M. Jääskeläinen are gratefully acknowledged. J.Z.B. is supported by the Massey University Research Fund. Additional funding was provided by the German Science Foundation (DFG) through SFB Transregio No. 12.

APPENDIX: DEFINITION OF AUXILIARY FUNCTIONS

Here we provide the six functions $\tilde{F}_n(\omega, \Delta_R, \Delta_I, \beta, \mu)$ (with $n = 1, \ldots, 6$) entering Eq. (12). We use the following abbreviations:

$$\epsilon_1(y) = \frac{1}{2}(\Delta_R - \sqrt{(\Delta_R - 2\Delta_I)^2 + 4y^2}),$$

$$\epsilon_2(y) = \frac{1}{2}(\Delta_R + \sqrt{(\Delta_R - 2\Delta_I)^2 + 4y^2}),$$

$$\epsilon_3(y) = \frac{1}{2}(-\Delta_R - \sqrt{(\Delta_R + 2\Delta_I)^2 + 4y^2}),$$

$$\epsilon_4(y) = \frac{1}{2}(-\Delta_R + \sqrt{(\Delta_R + 2\Delta_I)^2 + 4y^2}).$$

Furthermore, we define the quantities (setting here $\hbar = 1$ for simplicity)

$$y_1 = \frac{1}{2}\sqrt{-4\Delta_I^2 + 4\Delta_I\Delta_R - \Delta_R^2 + \omega^2},$$

$$y_2 = \frac{\sqrt{\omega}\sqrt{8\Delta_I^2\Delta_R - 2\Delta_R^3 - 4\Delta_I^2\omega + 5\Delta_R^2\omega - 4\Delta_R\omega^2 + \omega^3}}{\sqrt{4\Delta_R^2 - 8\Delta_R\omega + 4\omega^2}},$$

$$y_3 = \frac{\sqrt{-8\Delta_I^2\Delta_R\omega + 2\Delta_R^3\omega - 4\Delta_I^2\omega^2 + 5\Delta_R^2\omega^2 + 4\Delta_R\omega^3 + \omega^4}}{2\sqrt{\Delta_R^2 + 2\Delta_R\omega + \omega^2}},$$

$$y_4 = \frac{\sqrt{\omega}\sqrt{8\Delta_I^2\Delta_R - 2\Delta_R^3 - 4\Delta_I^2\omega + 5\Delta_R^2\omega - 4\Delta_R\omega^2 + \omega^3}}{\sqrt{4\Delta_R^2 - 8\Delta_R\omega + 4\omega^2}},$$

$$y_5 = \frac{\sqrt{\omega}\sqrt{8\Delta_I^2\Delta_R - 2\Delta_R^3 - 4\Delta_I^2\omega + 5\Delta_R^2\omega - 4\Delta_R\omega^2 + \omega^3}}{\sqrt{4\Delta_R^2 - 8\Delta_R\omega + 4\omega^2}},$$

$$y_6 = \frac{1}{2}\sqrt{-4\Delta_I^2 - 4\Delta_I\Delta_R - \Delta_R^2 + \omega^2}.$$

Finally, we define $\Delta_\pm = \Delta_R \pm 2\Delta_I$. With these conventions, the functions $\tilde{F}_n(\omega, \Delta_R, \Delta_I, \beta, \mu)$ can be expressed as follows:

$$\tilde{F}_1 = [f(\epsilon_1(y_1)) - f(\epsilon_2(y_1))]\frac{y_1\Delta_-^2}{16(4y_1^2 + \Delta_-^2)^{3/2}}\left|\frac{\sqrt{4y_1^2 + \Delta_-^2}}{y_1}\right|,$$

$$\tilde{F}_2 = [f(\epsilon_1(y_2)) - f(\epsilon_3(y_2))]\left|\frac{4y_2}{\sqrt{4y_2^2 + \Delta_-^2}} - \frac{4y_2}{\sqrt{4y_2^2 + \Delta_+^2}}\right|^{-1}\frac{y_2^3(-2\Delta_R + \sqrt{4y_2^2 + \Delta_-^2} - \sqrt{4y_2^2 + \Delta_+^2})}{(4y_2^2 + \Delta_-(\Delta_- - \sqrt{4y_2^2 + \Delta_-^2}))(4y_2^2 + \Delta_+(\Delta_+ + \sqrt{4y_2^2 + \Delta_+^2}))},$$

$$\tilde{F}_3 = [f(\epsilon_1(y_3)) - f(\epsilon_4(y_3))]\frac{y_3^2\sqrt{4y_3^2 + \Delta_-^2}\sqrt{4y_3^2 + \Delta_+^2}(-2\Delta_R + \sqrt{4y_3^2 + \Delta_-^2} + \sqrt{4y_3^2 + \Delta_+^2})}{4(\sqrt{4y_3^2 + \Delta_-^2} + \sqrt{4y_3^2 + \Delta_+^2})(4y_3^2 + \Delta_-(\Delta_- - \sqrt{4y_3^2 + \Delta_-^2}))(4y_3^2 + \Delta_+(\Delta_+ - \sqrt{4y^2 + \Delta_+^2}))},$$

$$\tilde{F}_4 = [f(\epsilon_2(y_4)) - f(\epsilon_3(y_4))]\frac{y_4^2\sqrt{4y_4^2 + \Delta_-^2}\sqrt{4y_4^2 + \Delta_+^2}(2\Delta_R + \sqrt{4y_4^2 + \Delta_-^2} + \sqrt{4y_4^2 + \Delta_+^2})}{4(\sqrt{4y_4^2 + \Delta_-^2} + \sqrt{4y_4^2 + \Delta_+^2})(4y_4^2 + \Delta_-(\Delta_- + \sqrt{4y_4^2 + \Delta_-^2}))(4y_4^2 + \Delta_+(\Delta_+ + \sqrt{4y_4^2 + \Delta_+^2}))},$$

$$\tilde{F}_5 = [f(\epsilon_2(y_5)) - f(\epsilon_4(y_5))]\left|\frac{4y_5}{\sqrt{4y_5^2 + \Delta_-^2}} - \frac{4y_5}{\sqrt{4y_5^2 + \Delta_+^2}}\right|^{-1}\frac{y_5^3(2\Delta_R + \sqrt{4y_5^2 + \Delta_-^2} - \sqrt{4y_5^2 + \Delta_+^2})}{(4y_5^2 + \Delta_-(\Delta_- + \sqrt{4y_5^2 + \Delta_-^2}))(4y_5^2 + \Delta_+(\Delta_+ - \sqrt{4y_5^2 + \Delta_+^2}))},$$

$$\tilde{F}_6 = [f(\epsilon_3(y_6)) - f(\epsilon_4(y_6))]\frac{y_6\Delta_+^2}{16(4y_6^2 + \Delta_+^2)^{3/2}}\left|\frac{\sqrt{4y_6^2 + \Delta_+^2}}{y_6}\right|.$$

[1] K. S. Novoselov, A. K. Geim, S. V. Morozov, D. Jiang, Y. Zhang, S. V. Dubonos, I. V. Grigorieva, and A. A. Firsov, Science **306**, 666 (2004).
[2] K. S. Novoselov, D. Jiang, F. Schedin, T. J. Booth, V. V. Khotkevich, S. V. Morosov, and A. K. Geim, Proc. Natl. Acad. Sci. U.S.A. **102**, 10451 (2005).
[3] P. R. Wallace, Phys. Rev. **71**, 622 (1947).
[4] C. Lee, X. Wei, J. W. Kysar, and J. Hone, Science **321**, 385 (2008).
[5] P. Avouris, Z. Chen, and V. Perebeinos, Nat. Nanotechnol. **2**, 605 (2007); Z. Chen, Y.-M. Lin, M. J. Rooks, and P. Avouris, Physica E **40**, 228 (2007); J. B. Oostinga, H. B. Heersche, X. Liu, A. F. Morpurgo, and L. M. K. Vandersypen, Nature Mater. **7**, 151 (2007).
[6] A. H. Castro Neto, F. Guinea, N. M. R. Peres, K. S. Novoselov, and A. K. Geim, Rev. Mod. Phys. **81**, 109 (2009).
[7] Y. Zhang, Y. Tan, H. L. Stormer, and P. Kim, Nature (London) **438**, 201 (2005).
[8] K. S. Novoselov, A. K. Geim, S. V. Morozov, D. Jiang, Y. Zhang, S. V. Dubonos, I. V. Grigorieva, and A. A. Firsov, Nature (London) **438**, 197 (2005).
[9] G. Dresselhaus and M. S. Dresselhaus, Phys. Rev. **140**, A401 (1965).
[10] T. Ando, J. Phys. Soc. Jpn. **69**, 1757 (2000).
[11] A. De Martino, R. Egger, K. Hallberg, and C. A. Balseiro, Phys. Rev. Lett. **88**, 206402 (2002).
[12] C. L. Kane and E. J. Mele, Phys. Rev. Lett. **95**, 226801 (2005).
[13] D. Huertas-Hernando, F. Guinea, and A. Brataas, Phys. Rev. B **74**, 155426 (2006).
[14] H. Min, J. E. Hill, N. A. Sinitsyn, B. R. Sahu, L. Kleinman, and A. H. MacDonald, Phys. Rev. B **74**, 165310 (2006).
[15] Y. Yao, F. Ye, X. L. Qi, S. C. Zhang, and Z. Fang, Phys. Rev. B **75**, 041401(R) (2007).
[16] J. C. Boettger and S. B. Trickey, Phys. Rev. B **75**, 121402(R) (2007).
[17] M. Zarea and N. Sandler, Phys. Rev. B **79**, 165442 (2009).
[18] D. Huertas-Hernando, F. Guinea, and A. Brataas, Phys. Rev. Lett. **103**, 146801 (2009).
[19] A. H. Castro Neto and F. Guinea, Phys. Rev. Lett. **103**, 026804 (2009).
[20] E. I. Rashba, Phys. Rev. B **79**, 161409(R) (2009).
[21] C. Ertler, S. Konschuh, M. Gmitra, and J. Fabian, Phys. Rev. B **80**, 041405(R) (2009).
[22] T. Stauber and J. Schliemann, New J. Phys. **11**, 115003 (2009).
[23] F. Kuemmeth and E. I. Rashba, Phys. Rev. B **80**, 241409(R) (2009).
[24] M. Gmitra, S. Konschuh, C. Ertler, C. Ambrosch-Draxl, and J. Fabian, arXiv:0904.3315 (unpublished).
[25] F. Kuemmeth, S. Ilani, D. C. Ralph, and P. L. McEuen, Nature (London) **452**, 448 (2008).
[26] Yu. S. Dedkov, M. Fonin, U. Rüdiger, and C. Laubschat, Phys. Rev. Lett. **100**, 107602 (2008).
[27] A. Varykhalov, J. Sanchez-Barriga, A. M. Shikin, C. Biswas, E. Vescovo, A. Rybkin, D. Marchenko, and O. Rader, Phys. Rev. Lett. **101**, 157601 (2008).
[28] O. Rader, A. Varykhalov, J. Sanchez-Barriga, D. Marchenko, A. Rybkin, and A. M. Shikin, Phys. Rev. Lett. **102**, 057602 (2009).
[29] A. Varykhalov and O. Rader, Phys. Rev. B **80**, 035437 (2009).
[30] N. Tombros, C. Jozsa, M. Popinciuc, H. T. Jonkman, and B. J. van Wees, Nature (London) **448**, 571 (2007).
[31] B. Trauzettel, D. V. Bulaev, D. Loss, and G. Burkard, Nat. Phys. **3**, 192 (2007).
[32] K. Ziegler, Phys. Rev. Lett. **97**, 266802 (2006).
[33] V. P. Gusynin, S. G. Sharapov, and J. P. Carbotte, Phys. Rev. Lett. **96**, 256802 (2006).
[34] K. Ziegler, Phys. Rev. B **75**, 233407 (2007).
[35] L. A. Falkovsky and A. A. Varlamov, Eur. Phys. J. B **56**, 281 (2007).
[36] N. M. R. Peres, T. Stauber, and A. H. Castro Neto, EPL **84**, 38002 (2008).
[37] E. J. Nicol and J. P. Carbotte, Phys. Rev. B **77**, 155409 (2008).
[38] C. Zhang, L. Chen, and Z. Ma, Phys. Rev. B **77**, 241402(R) (2008).
[39] V. P. Gusynin, S. G. Sharapov, and J. P. Carbotte, New. J. Phys. **11**, 095013 (2009).
[40] J. Z. Bernád, U. Zülicke, and K. Ziegler, Physica E (to be published).
[41] A. Yamakage, K.-I. Imura, J. Cayssol, and Y. Kuramoto, EPL **87**, 47005 (2009).
[42] A. R. Wright, G. X. Wang, W. Xuc, Z. Zeng, and C. Zhang, Microelectron. J. **40**, 857 (2009).
[43] O. Madelung, *Introduction to Solid-State Theory* (Springer, Berlin, 1978).
[44] C. L. Kane and E. J. Mele, Phys. Rev. Lett. **95**, 146802 (2005).
[45] L. Brey and H. A. Fertig, Phys. Rev. B **73**, 195408 (2006).
[46] C. Wu, B. A. Bernevig, and S.-C. Zhang, Phys. Rev. Lett. **96**, 106401 (2006).
[47] T. Giamarchi and H. J. Schulz, Phys. Rev. B **37**, 325 (1988).
[48] T. Giamarchi and A. J. Millis, Phys. Rev. B **46**, 9325 (1992).
[49] J. W. McClure, Phys. Rev. **108**, 612 (1957).
[50] A. G. Grushin, B. Valenzuela, and M. A. H. Vozmediano, Phys. Rev. B **80**, 155417 (2009).
[51] Z. Fei, Y. Shi, L. Pu, F. Gao, Y. Liu, L. Sheng, B. Wang, R. Zhang, and Y. Zheng, Phys. Rev. B **78**, 201402(R) (2008).
[52] K. F. Mak, M. Y. Sfeir, Y. Wu, C. H. Lui, J. A. Misewich, and T. F. Heinz, Phys. Rev. Lett. **101**, 196405 (2008).